Article

Not peer-reviewed version

Effective Medium Theory for Silica Nanoparticles

Feng Liu *, Yao Xu , Xiaowei Li

Posted Date: 25 November 2025

doi: 10.20944/preprints202511.1855.v1

Keywords: silica nanoparticles; effective medium theory; finite element simulation; anti-reflection coating; anti-glare coating

Article

Effective Medium Theory for Silica Nanoparticles

Feng Liu [1,2,3]*, Yao Xu [3] and Xiaowei Li [1]

[1] School of Materials Science and Physics, China University of Mining and Technology, Xuzhou 221-116, China
[2] Department of Physics, Shaoxing University, Shaoxing 312-000, China
[3] YongAn Optics (Nibgbo) co.ltd, Ningbo 312-000, China
* Correspondence: ruserzzz@gmail.com

Abstract

Silica nanoparticles are among the most commonly used materials for functional films. In this work, we develop an effective medium theory for randomly distributed silica nanoparticles with unshelled, shelled, mixed, and hollow spherical structures by incorporating Mie solutions. The proposed effective medium theory is validated against full-wave simulations performed using the finite-element method in three dimensional cases. Our results provide a practical tool for analyzing the optical properties of randomly distributed SNPs with diverse structures, facilitating the design of functional films such as anti-glare coatings.

Keywords: silica nanoparticles; effective medium theory; finite element simulation; anti-reflection coating; anti-glare coating

1. Introduction

Silica nanoparticles (SNPs), with radii typically ranging from 30 to 150 nanometers, are utilized in many fields, including drug delivery, battery anodes, and functional coatings [1–3]. Their tunable optical properties make them particularly suitable for fabricating anti-glare (anti-reflection) films [4]. In designing a multilayer anti-glare film, the effective dielectric constant is a critical material property [5]. Ideally, for a perfect anti-reflection coating, the dielectric constant $\varepsilon(d)$should vary continuously from that of the substrate to that of air, where d is the film thickness [6].

Various dielectric models for heterogeneous mixtures have been explored over the years, and summaries of these mixing formulas are available in the literature [7–10]. However, predicting the dielectric constant of SNP mixtures presents two main challenges. The first is the presence of strong surface plasmon resonances, particularly when a metallic shell is involved [11,12]. The second is the unavoidable size distribution of SNPs, which drastically alters the optical properties of the composite medium, especially when the particle radius approaches the wavelength of light. To address these issues, we incorporate Mie solutions into an effective medium theory (EMT) framework, such as the Clausius-Mossotti (CM) relation, and average the effective dielectric constant over the SNP radius distribution.

In this work, we develop an EMT for randomly distributed silica nanoparticles by combining the CM relation with Mie solutions for unshelled, shelled, mixed and hollow structures. We validate our EMT against numerical calculations performed with the finite-element method using the commercial software COMSOL Multiphysics. This EMT provides a tool for designing functional films by controlling the filling ratio and radius of SNPs with significantly reduced computational effort. The general concept of this work is illustrated in Figure 1.

 doi:10.20944/preprints202511.1855.v1

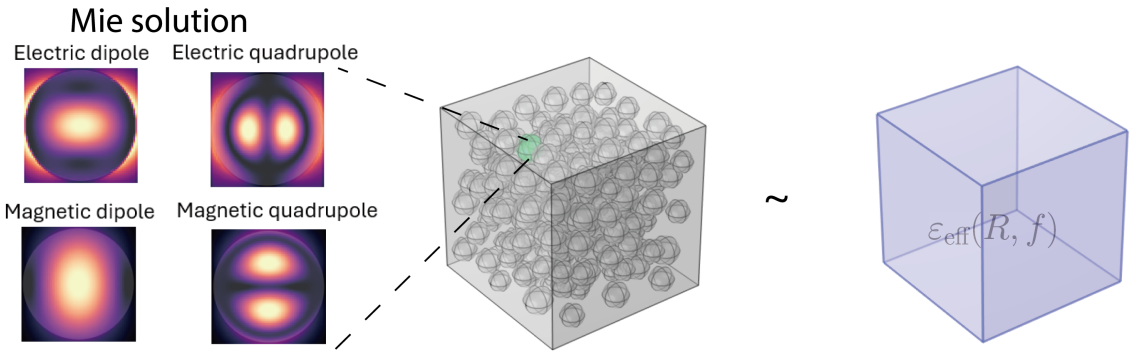

Figure 1. Schematic figure illustrating the concept of the work. Using Mie solution for approximating the effective polarizability of SNP, one can develop an effective uniform medium theory in terms of filling ratio and sphere radius.

The paper is organized as follows. In Section II, we begin with the classical CM relation, replace the polarizability with the Mie solution, and develop the EMT for unshelled, shelled, mixed and hollow SNP media. In Section III, we compare the reflection and transmission coefficients obtained from our EMT for all four structures with those from the finite-element simulations. A discussion and summary are provided in Section IV.

2. CM Relation and Mie Solutions

We begin with the well-known CM relation, which connects the effective dielectric constant ε_{eff} of two-component mixture to its local polarizability α as

$$\frac{\varepsilon_{\text{eff}} - \varepsilon_d}{\varepsilon_{\text{eff}} + 2\varepsilon_d} = \frac{f}{4\pi R^3 \varepsilon_0}\alpha, \tag{1}$$

where f and R are the filling ratio and mean radium of the SNPs. Substituting the static polarizability $\alpha = 4\pi\varepsilon_0 R^3 \frac{\varepsilon-1}{\varepsilon+2}$ into the Eq. (1) yields the widely used Maxwell-Garnett (MG) equation:

$$\varepsilon_{\text{eff}} = \frac{(2f+1)\varepsilon - 2f + 2}{(1-f)\varepsilon + 2 + f}. \tag{2}$$

Notably, the value of ε_{eff} in MG equation is irrelevant of the radius of SNPs. However, as the size of the SNPs increases, contributions from quadrupole and higher-order multipoles become significant. Furthermore, surface plasmon resonances cannot be ignored when a metallic shell is considered, as these effects depend critically on the ratio of the incident wavelength to the SNP radius.

2.1. Effective Polarizability

To address these limitations, we combine the Mie solution with the CM relation by replacing the local polarizability with an effective polarizability α_{eff}, defined such that:

$$\sigma_{\text{ext}} = \frac{k}{\varepsilon_0}\text{Im}(\alpha_{\text{eff}}), \tag{3}$$

where σ_{ext} is extinction cross-section, and $k = \frac{2\pi n_d}{\lambda}$ with n_d the refractive index of the medium and λ the wavelength of light. Within the Mie theory framework, the extinction cross-section is given by

$$\sigma_{\text{ext}} = \frac{2\pi R^2}{q^2}\text{Re}[\sum_n (2n+1)(a_n + b_n)], \tag{4}$$

 doi:10.20944/preprints202511.1855.v1

where a_n and b_n are the coefficients of Mie solution for electric and magnetic fields, respectively, n denotes the multipole expansion order such that $n = 1, 2$ for dipole and quadrupole terms, and $q = \frac{2\pi R n_d}{\lambda}$ is the size parameter.

Combining Eqs. (2) and (3) we obtain the effective polarizability in terms of Mie coefficients as

$$\alpha_{\text{eff}} = \frac{2\pi R^3 \varepsilon_0}{q^3} \sum_n i(2n+1)(a_n + b_n). \tag{5}$$

For an unshelled (homogeneous) sphere, the Mie coefficients a_n and b_n are given by

$$\begin{aligned} a_n &= \frac{n_1 \psi_n(q_1)\psi_n'(q) - \psi_n(q)\psi_n'(q_1)}{n_1 \psi_n(q_1)\zeta_n'(q) - \zeta_n(q)\psi_n'(q_1)}, \\ b_n &= \frac{\psi_n(q_1)\psi_n'(q) - n_1 \psi_n(q)\psi_n'(q_1)}{\psi_n(q_1)\zeta'(q) - n_1 \zeta_n(q)\psi_n'(q_1)}, \end{aligned} \tag{6}$$

where $q_1 = \frac{2\pi n_1 R}{\lambda}$ with n_1 the refractive index of the SNPs, and ψ_n, ζ_n are the spherical functions of Bessel and Hankel of the first kind, respectively. The Mie coefficients for a shelled structure (a core-shell particle) can be derived similarly and are expressed as [13]

$$\begin{aligned} a_n^{(2)} &= \frac{\psi_n(q)[\psi_n'(q_2) - A\kappa'(q_2)] - n_2 \psi_n'(q)[\psi_n(q_2) - A_n \kappa_n(q_2)]}{\zeta_n(q_2)[\psi_n'(q_w) - A\kappa'(q_2)] - n_2 \zeta_n'(q_2)[\psi_n(q_2) - A_n \kappa_n(q_2)]}, \\ b_n^{(2)} &= \frac{n_2 \psi(q)[\psi_n'(q_2) - B_n \kappa(q_2)] - \psi_n'(q)[\psi_n(q_2) - B_n \kappa_n(q_2)]}{n_2 \zeta_n(q)[\psi_n'(q_2) - B_n \zeta_n'(q_2)] - \zeta_n'(q)[\psi_n(q_2) - B_n \kappa_n(q_2)]}, \end{aligned} \tag{7}$$

where $q_2 = \frac{2\pi R_2 n_2}{\lambda}$ with n_2 and R_2 the refractive index and the radius of the shell, κ is the Bessel function of the second kind, and A_n, B_n are defined as

$$\begin{aligned} A_n &= \frac{n_2 \psi_n(n_2 q_1/n_1)\psi_n'(q_1) - n_1 \psi'(n_2 q_1/n_1)\psi_n(q_1)}{n_2 \kappa_n(n_2 q_1/n_1)\psi_n'(q_1) - n_1 \kappa_n'(n_2 q_1/n_1)\psi(q_1)}, \\ B_n &= \frac{n_2 \psi_n(q_1)\psi_n'(n_2 q_1/n_1) - n_1 \psi(n_2 q_1/n_1)\psi_n'(q_1)}{n_2 \kappa_n'(n_2 q_1/n_1)\psi_n(q_1) - n_1 \kappa_n(n_2 q_1/n_1)\psi_n'(q_1)}. \end{aligned} \tag{8}$$

These Mie coefficients are computed numerically [14]. The maximum order n for the multipole expansion is determined by the Wiscombe criterion, that is $n_{\text{cut}} = x + 4x^{1/3} + 2$ with $x = q$.

We now compare the local (static) polarizability with the effective polarizability derived from Mie theory for shelled and hollow structures. For a core-shell particle, the local polarizability in the electrostatic approximation is [11]

$$\alpha = 4\pi\varepsilon_0 R_2^3 \left[\frac{(\varepsilon_2 - \varepsilon_d)(\varepsilon_1 + 2\varepsilon_2) + f_R(\varepsilon_1 - \varepsilon_2)(\varepsilon_d + 2\varepsilon_2)}{(\varepsilon_2 + 2\varepsilon_d)(\varepsilon_1 + 2\varepsilon_2) + f_R(2\varepsilon_2 - \varepsilon_d)(\varepsilon_1 - \varepsilon_2)} \right] \tag{9}$$

where R_1 (ε_1) and R_2 (ε_2) are the radius (dielectric constant) of the core and shell, respectively, and $f_R = R_1^3/R_2^3$ is the volume ratio of core. The effective polarizability of shelled and hollow structures can be calculated by combining Eqs.(4) and (6).

Figure 2 shows a comparison between the polarizabilities obtained from the static approximation and the Mie solution for three different structures: unshelled spheres, silver-shelled spheres, and hollow spheres. The refractive indices of the host medium and the silica are set to 1.0 and 1.45, respectively. For the core-shell particles, the core radius is 80% of the shell radius. The dielectric function of silver is taken from experimental data [15]. As seen in Fig. 2, for a small size parameter R/λ (with $\lambda = 380$ nm), the local and effective polarizabilities agree well. A key distinction is that the effective polarizability possesses a non-zero imaginary part, which is absent in the local approximation.

 doi:10.20944/preprints202511.1855.v1

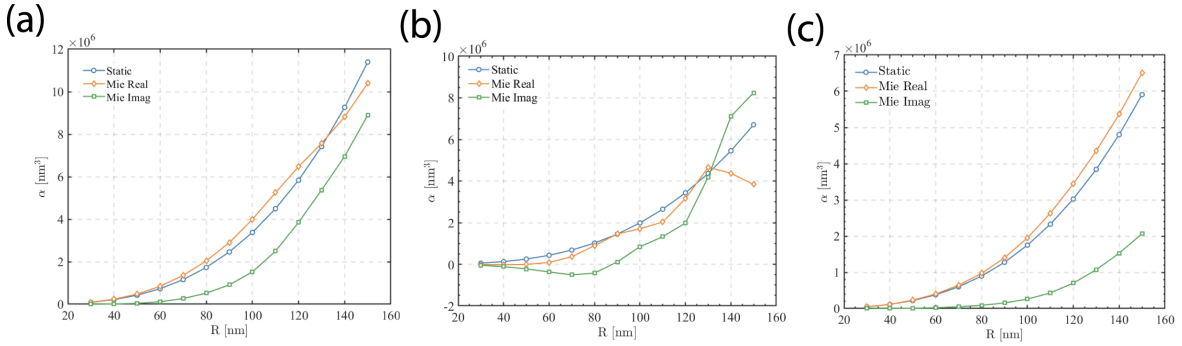

Figure 2. Comparison of effective polarizability of SNPs obtained by static approximation and Mie solution for (a) unshelled, (b) Ag-shelled and (c) hollow structures for different radii.

2.2. Effective Dielectric Constant

Using the effective polarizability α_{eff}, the effective dielectric constant can be calculated from the CM relation in Eq. (1), with α replaced by α_{eff}. In practice, SNPs synthesized via conventional routes exhibit a size distribution. To account for this, we model the distribution of radii R using a Gaussian function

$$P(R) = \frac{1}{2\pi\sigma^2} e^{-\frac{(x-\mu)^2}{2\sigma^2}}, \tag{10}$$

where μ is the mean value of R, and σ is the standard derivation. The effective dielectric constant is then averaged over this distribution as

$$\frac{\varepsilon_{\text{eff}} - \varepsilon_m}{\varepsilon_{\text{eff}} + 2\varepsilon_m} = \frac{f}{\langle R^3 \rangle} \int_{R_{\text{min}}}^{R_{\text{max}}} P(R')\alpha_{\text{eff}}(R')dR', \tag{11}$$

where R_{min} and R_{max} are the the lower and upper cutoff radii for the integration, and $\langle R^3 \rangle$ is the mean cubed radius. By substituting the Mie solution for α_{eff} and truncating the multipole expansion to include dipole and quadrupole terms, we obtain a working formula for the effective dielectric constant

$$\varepsilon_{\text{eff}} = 1 - 3f \int_{R_{\text{min}}}^{R_{\text{max}}} P(R) \frac{3(a_1 + b_1) + 5(a_2 + b_2)}{2iq^3 + f(3(a_1 + b_1) + 5(a_2 + b_2))} dR, \tag{12}$$

where q takes q_2 for the shelled structure, and we set $\varepsilon_d = 1$.

The calculated real part of the effective dielectric constant for unshelled, Ag-shelled, mixed, and hollow SNPs is plotted in Fig. 3 for different wavelengths. The filling ratio is 0.25, and the mean radius of the SNPs is 35 nm, and $\sigma = 3$ nm. R_{min} and R_{max} are set as 10 nm and 50 nm, respectively. The dielectric constant of host medium is set as 1.0. The integration was performed with 5000 sampling points. For the mixed structure, we set the ratio between unshelled and silver-shelled spheres is 1:1. Figure 3 shows that the dielectric function decreases monotonically with increasing wavelength for unshelled and hollow structures. In contrast, for the silver-shelled and mixed structures, distinct singularities appear near 600 nm and 550 nm, respectively, due to plasmon resonances.

 doi:10.20944/preprints202511.1855.v1

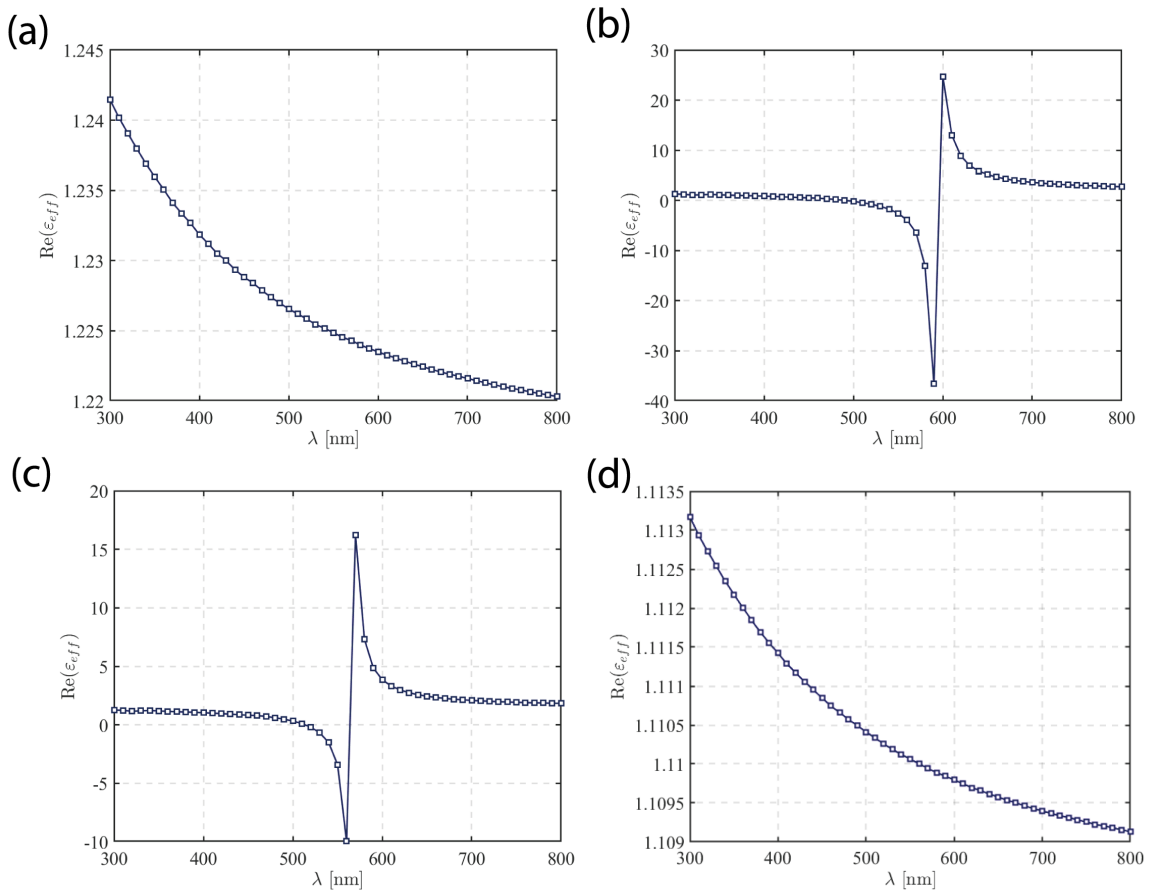

Figure 3. Effective dielectric functions obtained by Mie solution of SNPs for (a) unshelled, (b) Ag-shelled, (c) mixed and (d) hollow structures for different wavelengths.

3. Validation of EMT

We now validate our EMT by comparing its predictions for reflectance and transmittance with results from full-wave finite-element method simulations as displayed in Figure 4. The simulation geometry with meshed structure is shown in the inset of Fig. 4(e): incident light propagates along the z-direction with the electric field polarized along the x-axis.m, and periodic boundary conditions are adopted along x- and y-directions.

 doi:10.20944/preprints202511.1855.v1

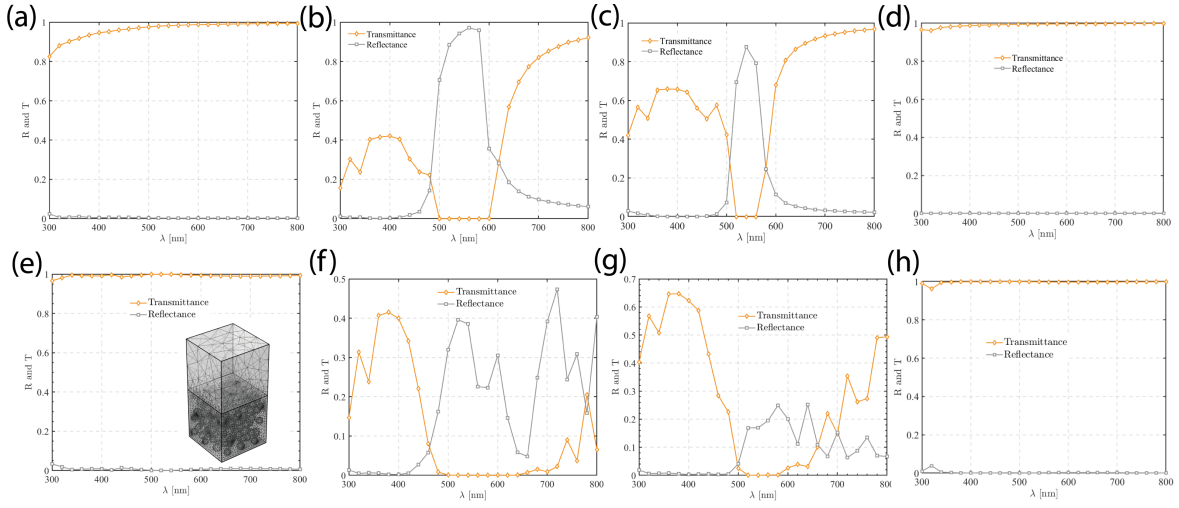

Figure 4. Reflectance and Transmittance of SNPs at different wavelengths calculated by the effective medium theory for (a) unshelled, (b) Ag-shelled, (c) mixed and (d) hollow structures. (e) – (h) similar to (a) – (d) calculated by the finite element method. Inset of (e) is the mesh structure of the finite element simulation.

Figure 4(a)-(d) shows that the EMT, based on Mie solutions, generally reproduces the trends in the finite-element method results, particularly for the unshelled and hollow structures. For the Ag-shelled structure, the finite-element method results [Figure 4(e) to (h)] exhibit several resonance peaks at wavelengths longer than 500 nm, which are not fully captured by the EMT. This discrepancy may be attributed to finite-size effects and spatial correlations between particles in the FEM simulation, which are not accounted for in the quasi-static, mean-field EMT.

4. Summary

We have developed an effective medium theory for silica nanoparticles by integrating Mie solutions with the Clausius-Mossotti relation. This theory calculates the effective polarizability using the full set of Mie coefficients, incorporating both electric and magnetic multipole contributions. We applied this framework to three types of structures: unshelled spheres, Ag-shelled spheres, and hollow spheres. The transmittance and reflectance predicted by our effective medium theory were compared with those from finite-element simulations, showing good agreement for non-plasmonic structures and capturing the overall behavior for plasmonic ones. Our results provide a practical and computationally efficient tool for analyzing the optical properties of silica nanoparticles with various structures, aiding in the rational design of functional films for applications such as anti-glare coatings.

Author Contributions: Y. Xu initial the project, F. Liu and X.-W. Li conceptualize the core idea. All authors contribute to the composition of the manuscript.

Funding: This research received no external funding.

Data Availability Statement: The authors will supply the relevant data in response to reasonable requests.

Conflicts of Interest: The authors declare no conflicts of interest.

References

1. Sharma, J.; Polizos, G. Hollow Silica Particles: Recent Progress and Future Perspectives. *Nanomater.* **2020**, *10*.
2. Janjua, T.I.; Cao, Y.; Kleitz, F.; Linden, M.; Yu, C.; Popat, A. Silica nanoparticles: A review of their safety and current strategies to overcome biological barriers. *Adv. Drug Deliv. Rev.* **2023**, *203*, 115115. https://doi.org/https://doi.org/10.1016/j.addr.2023.115115.
3. Saha, A.; Mishra, P.; Biswas, G.; Bhakta, S. Greening the pathways: a comprehensive review of sustainable synthesis strategies for silica nanoparticles and their diverse applications. *RSC Adv.* **2024**, *14*, 11197–11216. https://doi.org/10.1039/D4RA01047G.

 doi:10.20944/preprints202511.1855.v1

4. Tao, C.; Zou, X.; Du, K.; Zhang, L.; Yan, H.; Yuan, X. Ultralow-refractive-index optical thin films built from shape-tunable hollow silica nanomaterials. *Opt. Lett.* **2018**, *43*, 1802–1805. https://doi.org/10.1364/OL.43.001802.
5. Hiller, J.; Mendelsohn, J.D.; Rubner, M.F. Reversibly erasable nanoporous anti-reflection coatings from polyelectrolyte multilayers. *Nat. Mater.* **2002**, *1*, 59–63. https://doi.org/10.1038/nmat719.
6. Raut, H.K.; Ganesh, V.A.; Nair, A.S.; Ramakrishna, S. Anti-reflective coatings: A critical, in-depth review. *Energy Environ. Sci.* **2011**, *4*, 3779–3804. https://doi.org/10.1039/C1EE01297E.
7. Sihvola, A. *Electromagnetic Mixing Formulas and Applications*; The Institution of Engineering and Technology: London, 1999.
8. Félidj, N.; Aubard, J.; Lévi, G. Discrete dipole approximation for ultraviolet–visible extinction spectra simulation of silver and gold colloids. *J. Chem. Phys.* **1999**, *111*, 1195–1208. https://doi.org/10.1063/1.479305.
9. Foldy, L.L. The multiple scattering of waves. I. General theory of isotropic scattering by randomly distributed scatterers. *Phys. Rev.* **1945**, *67*, 107–119. https://doi.org/10.1103/PhysRev.67.107.
10. Maier, S.A. *Plasmonics: Fundamentals and Applications*; Springer: New York, 2007.
11. Malasi, A.; Kalyanaraman, R.; Garcia, H. From Mie to Fresnel through effective medium approximation with multipole contributions. *J. Opt.* **2014**, *16*, 065001. https://doi.org/10.1088/2040-8978/16/6/065001.
12. Colom, R.; Devilez, A.; Enoch, S.; Stout, B.; Bonod, N. Polarizability expressions for predicting resonances in plasmonic and Mie scatterers. *Phys. Rev. A* **2017**, *95*, 063833. https://doi.org/10.1103/PhysRevA.95.063833.
13. Zhong-cai, Y.; Jia-ming, S.; Jia-chun, W.; Ji-wei, X. Validity of effective-medium theory in Mie scattering calculation of hollow dielectric sphere. In Proceedings of the 2006 7th International Symposium on Antennas, Propagation & EM Theory, 2006, pp. 1–4. https://doi.org/10.1109/ISAPE.2006.353552.
14. Schäfer, J.; Lee, S.C.; Kienle, A. Calculation of the near fields for the scattering of electromagnetic waves by multiple infinite cylinders at perpendicular incidence. *J. Quant. Spectrosc. Radiat. Transf.* **2012**, *113*, 2113–2123. https://doi.org/https://doi.org/10.1016/j.jqsrt.2012.05.019.
15. Ciesielski, A.; Skowronski, L.; Trzcinski, M.; Szoplik, T. Controlling the optical parameters of self-assembled silver films with wetting layers and annealing. *Appl. Surf. Sci.* **2017**, *421*, 349–356. https://doi.org/https://doi.org/10.1016/j.apsusc.2017.01.039.